Exclusive photoproduction of J/ψ in proton-proton and proton-antiproton scattering

W. Schäfer[1,*] and A. Szczurek[1,2,†]

[1]*Institute of Nuclear Physics PAN, PL-31-342 Cracow, Poland*

[2]*University of Rzeszów, PL-35-959 Rzeszów, Poland*

(Received 22 May 2007; published 13 November 2007)

Protons and antiprotons at collider energies are a source of high-energy Weizsäcker-Williams photons. This may open a possibility to study exclusive photoproduction of heavy vector mesons at energies much larger than possible at the HERA accelerator. Here we present a detailed investigation of the exclusive J/ψ photoproduction in proton-proton (Relativistic Heavy Ion Collider, CERN LHC) and proton-antiproton (Tevatron) collisions. We calculate several differential distributions in t_1, t_2, y, ϕ, as well as transverse momentum distributions of J/ψ's. We discuss correlations in the azimuthal angle between outgoing protons or proton and antiproton as well as in the (t_1, t_2) space. Differently from electroproduction experiments, here both colliding beam particles can be a source of photons, and we find large interference terms in azimuthal-angle distributions in a broad range of rapidities of the produced meson. We also include the spin-flip parts in the electromagnetic vertices. We discuss the effect of absorptive corrections on various distributions. Interestingly, absorption corrections induce a charge asymmetry in rapidity distributions, and are larger for pp reactions than for the $p\bar{p}$ case. The reaction considered here constitutes an important nonreduceable background in recently proposed searches for odderon exchange.

DOI: 10.1103/PhysRevD.76.094014 PACS numbers: 13.87.Ce, 13.60.Le, 13.85.Lg

I. INTRODUCTION

The diffractive photoproduction of J/ψ mesons has recently been a subject of thorough studies at HERA [1,2], and serves to elucidate the physics of the QCD pomeron and/or the small-x gluon density in protons (for a recent review and references, see [3]). Being charged particles, protons/antiprotons available at e.g. the Relativistic Heavy Ion Collider (RHIC), Tevatron, and CERN LHC are a source of high-energy Weizsäcker-Williams photons, and photoproduction processes are also accessible in hadronic collisions. Hadronic exclusive production mechanisms of mesons at central rapidities in pp collisions were intensively studied in the 1990s at energies of a few tens of GeV [4], and raised much theoretical interest for their potential of investigating exotic hadronic states (see e.g. [5]). Recently there was interest in describing diffractive exclusive production of heavy scalar [6,7] and pseudoscalar [8] mesons in terms of off-diagonal unintegrated gluon distributions, which may provide insight into the related diffractive production mechanism of the Higgs boson ([9,10] and references therein). A purely hadronic mechanism for the exclusive production of J/ψ mesons in proton-proton and proton-antiproton collisions was suggested as a candidate in searches for yet another exotic object of QCD, the elusive odderon exchange [11,12]. In order to identify the odderon exchange, one has to consider all other possible processes leading to the same final channel which in the context of the searches for the odderon will constitute the unwanted background. One such process (and perhaps the only one at the level of fully exclusive J/ψ production) is pomeron-photon or photon-pomeron fusion [12–14], which we study in this communication on a more detailed level than available in the literature. We feel that its role as a background for odderon searches warrants a more detailed analysis, including energy dependence and differential distributions of the photoproduction mechanism in hadronic collisions. As will be discussed, the process considered here is also interesting in its own right. For information about ongoing experimental analysis at Tevatron and a discussion of prospects for LHC, see for example [15].

An important concern of our work are absorption effects. More often than not absorption effects are either completely ignored or included as a multiplicative reduction factor, which is simply wrong for many observables (like distributions in t_1 or t_2), as we shall show in our paper. We think this point requires broader public spread as it often appears to be forgotten or ignored. We present a detailed analysis of several differential distributions in order to identify the absorption effects. We also put special emphasis on interference phenomena. We will discuss more subtle phenomena as well, like the spin flip in the electromagnetic vertices and a charge asymmetry, by comparing differential distributions in proton-proton and proton-antiproton exclusive J/ψ production.

In this work, we do not include a possible odderon contribution. We wish to stress that the photoproduction mechanism of exclusive J/ψ's must exist without doubt, and does not die out as energy increases. A related purely hadronic (odderon) contribution with the same properties has not been unambiguously identified in other experiments, and hence cannot be estimated in a model-independent way. While certain QCD-inspired toy models for C-odd multigluon t-channel exchanges exist, they do

*Wolfgang.Schafer@ifj.edu.pl
†Antoni.Szczurek@ifj.edu.pl

not allow reliable calculations of hadronic amplitudes. In practice, the magnitude of the corresponding Born amplitude strongly depends on the details of how to treat gluons in the nonperturbative domain, as well as on the modeling of proton structure. Furthermore, the energy dependence of the full (beyond the Born approximation, and beyond perturbation theory) amplitude is unknown and it cannot be excluded that this contribution would even vanish with rising energy. It is not the issue of our paper to further discuss such models; we rather think that in the search for an odderon one should take further initiative, if substantial deviations from the more conservative physics discussed here are found.

II. AMPLITUDES AND CROSS SECTIONS

A. 2 → 3 amplitude

Here we present the necessary formalism for the calculation of amplitudes and cross sections. The basic mechanisms are shown in Fig. 1.

The distinctive feature, when compared to photoproduction in lepton-hadron collisions, is that now both participating hadrons can serve as the source of the photon, and it is necessary to take account of the interference between the two amplitudes. Because of the Coulomb singularities in the photon-exchange parts of the amplitude, the electromagnetic vertices involve only very small, predominantly transverse momentum transfers. Their effect is fully quantified by the well-known electromagnetic Dirac and Pauli form factors of the nucleon. Regarding the photoproduction amplitude, we try to be as far as possible model independent, and take advantage of the precise knowledge of diffractive vector-meson production over a broad energy range available from experiments at HERA. The amplitude for the $2 \to 3$ process of Fig. 1 can be decomposed as

$$\begin{aligned}
&\mathcal{M}^{\lambda_1\lambda_2\to\lambda_1'\lambda_2'\lambda_V}_{h_1h_2\to h_1h_2V}(s, s_1, s_2, t_1, t_2) \\
&= \mathcal{M}_{\gamma\mathbb{P}} + \mathcal{M}_{\mathbb{P}\gamma} \\
&= \langle p_1', \lambda_1'|J_\mu|p_1, \lambda_1\rangle \epsilon^*_\mu(q_1, \lambda_V)\frac{\sqrt{4\pi\alpha_{\rm em}}}{t_1} \\
&\quad\times \mathcal{M}^{\lambda_{\gamma^*}\lambda_2\to\lambda_V\lambda_2}_{\gamma^*h_2\to Vh_2}(s_2, t_2, Q_1^2) + \langle p_2', \lambda_2'|J_\mu|p_2, \lambda_2\rangle \\
&\quad\times \epsilon^*_\mu(q_2, \lambda_V)\frac{\sqrt{4\pi\alpha_{\rm em}}}{t_2}\,\mathcal{M}^{\lambda_{\gamma^*}\lambda_1\to\lambda_V\lambda_1}_{\gamma^*h_1\to Vh_1}(s_1, t_1, Q_2^2). \qquad (2.1)
\end{aligned}$$

The outgoing protons lose only tiny fractions $z_1, z_2 \ll 1$ of their longitudinal momenta. In terms of their transverse momenta $\boldsymbol{p}_{1,2}$ the relevant four-momentum transfers squared are $t_i = -(\boldsymbol{p}_i^2 + z_i^2 m_p^2)/(1 - z_i)$, $i = 1, 2$, and $s_1 \approx (1 - z_2)s$ and $s_2 \approx (1 - z_1)s$ are the familiar Mandelstam variables for the appropriate subsystems. Because of the smallness of the photon virtualities, denoted by $Q_i^2 = -t_i$,[1] it is justified to neglect the contribution from longitudinal photons; recall that $\sigma_L(\gamma^* p \to J/\psi p)/\sigma_T(\gamma^* p \to J/\psi p) \propto Q^2/m_{J/\psi}^2$ [2,3]. Then, the amplitude for emission of a photon of transverse polarization λ_V, and transverse momentum $\boldsymbol{q}_1 = -\boldsymbol{p}_1$, entering Eq. (2.1) reads

$$\begin{aligned}
&\langle p_1', \lambda_1'|J_\mu|p_1, \lambda_1\rangle \epsilon^*_\mu(q_1, \lambda_V) \\
&= \frac{(\boldsymbol{e}^{*(\lambda_V)}\boldsymbol{q}_1)}{\sqrt{1 - z_1}}\,\frac{2}{z_1}\,\chi^\dagger_{\lambda'}\left\{F_1(Q_1^2) - \frac{i\kappa_p F_2(Q_1^2)}{2m_p}(\boldsymbol{\sigma}_1 \cdot [\boldsymbol{q}_1, \boldsymbol{n}])\right\}\chi_\lambda. \qquad (2.2)
\end{aligned}$$

Here $\boldsymbol{e}^{(\lambda)} = -(\lambda\boldsymbol{e}_x + i\boldsymbol{e}_y)/\sqrt{2}$, $\boldsymbol{n}||\boldsymbol{e}_z$ denotes the collision axis, $\boldsymbol{\sigma}_1/2$ is the spin operator for nucleon 1, and χ_λ is its spinor. F_1 and F_2 are the Dirac and Pauli electromagnetic form factors, respectively. Here we have given only that part of the current which gives rise to the logarithmic dz/z longitudinal momentum spectrum of photons, which dominates in the high-energy kinematics considered here. It is worthwhile to recall that, for a massive fermion, which includes a spin-flip contribution originating from its anomalous magnetic moment, $\kappa_p = 1.79$. Notice its suppression at small transverse momenta. The parametrization of the photoproduction amplitude which we used in practical calculations can be found in the Appendix. Above, we already used the assumption of s-channel-helicity conservation in the $\gamma^* \to J/\psi$ transition, which for heavy vector mesons is indeed well justified by experiment[2] [1–3]. In summary we present the $2 \to 3$ amplitude in the form of a 2-dimensional vector as

$$\begin{aligned}
\boldsymbol{M}(\boldsymbol{p}_1, \boldsymbol{p}_2) &= e_1\frac{2}{z_1}\frac{\boldsymbol{p}_1}{t_1}\mathcal{F}_{\lambda_1'\lambda_1}(\boldsymbol{p}_1, t_1)\mathcal{M}_{\gamma^*h_2\to Vh_2}(s_2, t_2, Q_1^2) \\
&\quad + e_2\frac{2}{z_2}\frac{\boldsymbol{p}_2}{t_2}\mathcal{F}_{\lambda_2'\lambda_2}(\boldsymbol{p}_2, t_2)\mathcal{M}_{\gamma^*h_1\to Vh_1}(s_1, t_1, Q_2^2). \qquad (2.3)
\end{aligned}$$

The differential cross section of interest is given in terms of $\boldsymbol{M}$ as

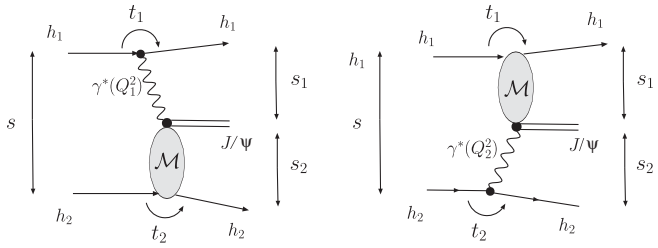

FIG. 1. The sketch of the two mechanisms considered in the present paper: $\gamma\mathbb{P}$ (left panel) and $\mathbb{P}\gamma$ (right panel). In addition, some kinematical variables are shown.

[1]Of course here the notation $Q_i^2 = t_i$ applies only to the photon lines.

[2]While a trend towards s-channel-helicity violating effects may be visible in the H1 data [2], they are surely negligible for our purpose, and within error bars, consistent with [1] and s-channel-helicity conservation.

$$d\sigma = \frac{1}{512\pi^4 s^2}|\boldsymbol{M}|^2 dy dt_1 dt_2 d\phi, \tag{2.4}$$

where $y \approx \log(z_1\sqrt{s}/m_{J/\Psi})$ is the rapidity of the vector meson, and ϕ is the angle between $\boldsymbol{p}_1$ and $\boldsymbol{p}_2$. Notice that the interference between the two mechanisms $\gamma\mathbb{P}$ and $\mathbb{P}\gamma$ is proportional to $e_1 e_2(\boldsymbol{p}_1 \cdot \boldsymbol{p}_2)$ and introduces a charge asymmetry as well as an angular correlation between the outgoing protons. Clearly, the interference cancels out after integrating over ϕ, and the integrated distributions will coincide for pp and $p\bar{p}$ collisions.

B. Absorptive corrections

We still need to correct for a major omission in our description of the production amplitude. Consider, for example, a rest frame of proton 2 (the target) in the left panel of Fig. 1. Here, the virtual photon may be viewed as a parton of proton 1 (the beam), separated from it by a large distance in impact parameter space. It splits into its $c\bar{c}$-Fock component at a large longitudinal distance before the target, and to obtain the sought for production amplitude we project the elastically scattered $c\bar{c}$ system onto the desired J/ψ final state [16]. We entirely neglected the possibility [17] that the photon's spectator partons might participate in the interaction and destroy the rapidity gap(s) in the final state. Stated differently, for the diffractive final state of interest, spectator interactions do not cancel and will affect the cross section. As a QCD mechanism, consider the interaction of a $\{c\bar{c}\}_1\{qqq\}_1$-beam system with the target by multiple gluon exchanges (see Fig. 2). Then, for the J/ψ final state of interest, the interaction of the $c\bar{c}$-color-singlet state is dominated by small dipole sizes $r_s \sim 4/m_{J/\psi}$ (the scanning radius of [18]). It can be exhausted by the minimal two-gluon color-singlet exchange, and will be quantified by the color-dipole cross section $\sigma(\boldsymbol{r})$ [16,19], respectively, its nonforward generalization [20,21]. Let $\boldsymbol{b}_V$ be the transverse separation of J/ψ and the target, and $\boldsymbol{r}$ the size of the $c\bar{c}$ dipole as shown in Fig. 2. Then, the $2 \to 3$ amplitude of Sec. II A will involve, besides the vertex for the $p \to \gamma p$ transition, the expectation value $\langle J/\psi|\Gamma^{(0)}(\boldsymbol{r}, \boldsymbol{b}_V)|\gamma\rangle$ of

$$\Gamma^{(0)}(\boldsymbol{r}, \boldsymbol{b}_V) = \tfrac{1}{2}\sigma(\boldsymbol{r}) t_N(\boldsymbol{b}_V, B), \tag{2.5}$$

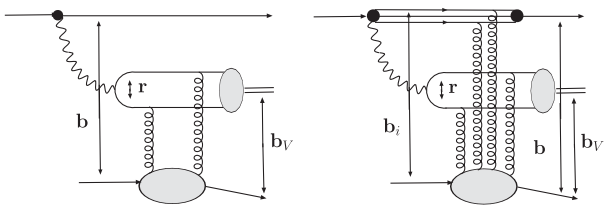

FIG. 2. Left panel: the QCD two-gluon exchange mechanism for the Born-level amplitude. Right panel: a possible multigluon-exchange contribution that involves uncanceled spectator interactions. The impact parameters relevant for the discussion are indicated.

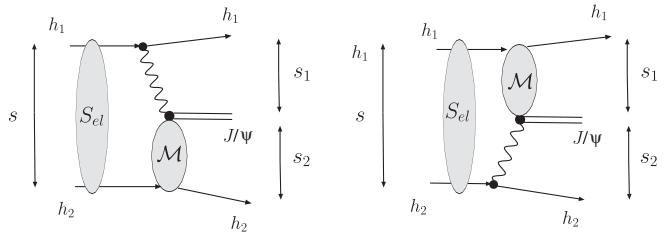

FIG. 3. A sketch of the elastic rescattering amplitudes effectively taken into account by Eq. (2.7).

where $t_N(\boldsymbol{b}, B) = \exp(-\boldsymbol{b}^2/2B)/(2\pi B)$ is an optical density of the target. A systematic account of the spectator interactions in QCD, however, is a difficult problem, as one cannot rely on the Abramovsky-Gribov-Kancheli (AGK) [22] cutting rules, when due account for color is taken [23]. To obtain at least a qualitative account of absorptive corrections, we restrict ourselves to only a subclass of absorptive corrections, the "diffractive cut," whose contribution is model independent [24]. Regarding our $\{c\bar{c}\}_1\{qqq\}_1$ system, with $\boldsymbol{b}_i$ denoting the constituent quarks' impact parameters, and $\boldsymbol{b}$ the impact parameter of the beam proton, the absorbed amplitude in impact parameter space will contain

$$\begin{aligned}\Gamma(\boldsymbol{r}, \boldsymbol{b}_V, \boldsymbol{b}) &= \tfrac{1}{2}\sigma(\boldsymbol{r}) t_N(\boldsymbol{b}_V, B) - \tfrac{1}{4}\sigma(\boldsymbol{r})\sigma_{qqq}(\{\boldsymbol{b}_i\}) t_N(\boldsymbol{b}_V, B) \\ &\quad \times t_N(\boldsymbol{b}, B_{\rm el}) \\ &= \Gamma^{(0)}(\boldsymbol{r}, \boldsymbol{b}_V)(1 - \tfrac{1}{2}\sigma_{qqq}(\{\boldsymbol{b}_i\}) t_N(\boldsymbol{b}, B_{\rm el})) \\ &\to \Gamma^{(0)}(\boldsymbol{r}, \boldsymbol{b}_V) \cdot S_{\rm el}(\boldsymbol{b}). \end{aligned} \tag{2.6}$$

In effect, we merely multiply the Born-level amplitude $\Gamma^{(0)}$ by the probability amplitude for the beam and target to pass through each other without inelastic interaction. In momentum space, we obtain the absorbed amplitude depicted in Fig.3 as

$$\begin{aligned}\boldsymbol{M}(\boldsymbol{p}_1, \boldsymbol{p}_2) &= \int \frac{d^2\boldsymbol{k}}{(2\pi)^2} S_{\rm el}(\boldsymbol{k}) \boldsymbol{M}^{(0)}(\boldsymbol{p}_1 - \boldsymbol{k}, \boldsymbol{p}_2 + \boldsymbol{k}) \\ &= \boldsymbol{M}^{(0)}(\boldsymbol{p}_1, \boldsymbol{p}_2) - \delta\boldsymbol{M}(\boldsymbol{p}_1, \boldsymbol{p}_2), \end{aligned} \tag{2.7}$$

and with

$$\begin{aligned} S_{\rm el}(\boldsymbol{k}) &= (2\pi)^2 \delta^{(2)}(\boldsymbol{k}) - \tfrac{1}{2}T(\boldsymbol{k}), \\ T(\boldsymbol{k}) &= \sigma_{\rm tot}^{pp}(s) \exp(-\tfrac{1}{2}B_{\rm el}\boldsymbol{k}^2), \end{aligned} \tag{2.8}$$

the absorptive correction $\delta\boldsymbol{M}$ reads[3]

$$\delta\boldsymbol{M}(\boldsymbol{p}_1, \boldsymbol{p}_2) = \int \frac{d^2\boldsymbol{k}}{2(2\pi)^2} T(\boldsymbol{k}) \boldsymbol{M}^{(0)}(\boldsymbol{p}_1 - \boldsymbol{k}, \boldsymbol{p}_2 + \boldsymbol{k}). \tag{2.9}$$

[3]In the practical calculations below, for Tevatron energies, we take $\sigma_{\rm tot}^{p\bar{p}} = 76$ mb, $B_{\rm el} = 17$ GeV^{-2} [25].

A number of improvements on this result can be expected to be relevant. First, a more consistent microscopic treatment of spectator interactions along the lines of [23] would be desirable. Experience from hadronic phenomenology [26] suggests that, at Tevatron energies, the purely elastic rescattering taken into account by Eq. (2.9) is insufficient, and inelastic screening corrections will to a crude estimate lead to an enhancement of absorptive corrections by a factor $\lambda \sim (\sigma_{\rm el} + \sigma_D)/\sigma_{\rm el}$ [27]. Here $\sigma_D = 2\sigma_{\rm SD} + \sigma_{\rm DD}$, and $\sigma_{\rm SD} = \sigma(pp \to pX)$, $\sigma_{\rm DD} = \sigma(pp \to XY)$ are the cross sections for single- and double-diffractive processes, respectively. Second, the $\gamma p \to J/\psi p$ production amplitude will also be affected by unitarity corrections. For example, with the increasing rapidity gap Δy between J/ψ and the target, one should account for additional s-channel gluons, and for sufficiently dense multiparton systems, the two-gluon exchange approximation for the $\gamma \to J/\psi$ transition used above ultimately becomes inadequate. For relevant discussions of unitarity/saturation effects in diffractive J/ψ production, see [28]; the scaling properties of vector-meson production in the presence of a large saturation scale are found in [21]. In our present approach, where the production amplitude is taken essentially from experiment, one must content oneself with the fact that (some) saturation effects are effectively contained in our parametrization, and any extrapolation beyond the energy domain covered by data must be taken with great caution.

III. RESULTS

In this section we shall present results of differential cross sections for J/ψ production. We shall concentrate on the Tevatron energy $W = 1960$ GeV, where such a measurement might be possible even at present. While in this paper we concentrate on the fully exclusive process $pp \to ppJ/\psi$, $p\bar{p} \to p\bar{p}J/\psi$, it is important to realize that from an experimental point of view there are additional contributions related to the exclusive production of χ_c mesons and their subsequent radiative decays to $J/\psi\gamma$. It may be difficult to measure/resolve the soft decay photons, and therefore experimentally this contribution may be seen as exclusive production of J/ψ. We note in this context that besides the scalar $\chi_c(0^{++})$ meson, whose exclusive production has been discussed in the literature (e.g. [6,7] and references therein), the axial-vector and tensor states $\chi_c(1^{++})$ and $\chi_c(2^{++})$ have larger branching fractions into the relevant $J/\psi\gamma$ channel. Although their exclusive production cross sections can be expected to be suppressed at low transverse momenta [6,29], a more detailed numerical analysis does not exist in the literature and would clearly go beyond the scope of the present paper. We note, however, that in Ref. [7] the cross section for exclusive production of $J/\psi\gamma$ from $\chi_c(0^{++})$ decays has been estimated to be $0.1 \div 5$ nb, which is much smaller than the photoproduction cross section of J/ψ discussed in this work, which is on the order of $20 \div 24$ nb.

A. Distributions of J/ψ

Let us start from the rapidity distribution of J/ψ shown in Fig. 4. In this figure we also present the subsystem energies $\sqrt{s_1}$, $\sqrt{s_2}$. At $|y| > 3$ the energies of the $\gamma p \to J/\psi p$ or $\gamma\bar{p} \to J/\psi\bar{p}$ subprocesses exceed the energy range explored at HERA. This may open a possibility to study J/ψ photoproduction at Tevatron. This is interesting by itself and requires further detailed studies. In turn, this means that our estimate of the cross section far from the midrapidity region requires extrapolations above the measured energy domain. In Fig. 5 we collect rapidity distributions for different energies relevant for the RHIC, Tevatron, and LHC. We observe an occurrence of a small dip in the distribution at midrapidities at LHC energy. The shape of the rapidity distribution at LHC energies, however, relies precisely on the above-mentioned extrapolation of the parametrization of HERA data to higher energies. Clearly a real experiment at the Tevatron and the LHC would help to constrain cross sections for the $\gamma p \to J/\psi p$ process.

In order to understand the origin of the small dip at midrapidity at LHC energy, in Fig. 6 we show separately the contributions of the two components ($\gamma\mathbb{P}$, $\mathbb{P}\gamma$ exchange) for the Tevatron (left panel) and the LHC (right panel). We see that at LHC energy the two components become better separated in rapidity. This reflects the strong rise of the J/ψ photoproduction cross section with energy, which can be expected to slow down with increasing energy. Notice that the beam hadron h_1 moves along

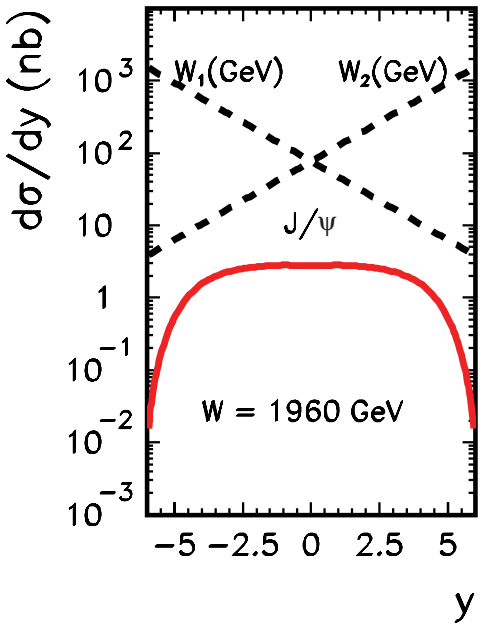

FIG. 4 (color online). $d\sigma/dy$ as a function of the J/ψ rapidity (y) for W = 1960 GeV. For a better understanding of the results we also show (dashed lines) the subsystem energies $W_{1V} = \sqrt{s_1}$ and $W_{2V} = \sqrt{s_2}$ in GeV.

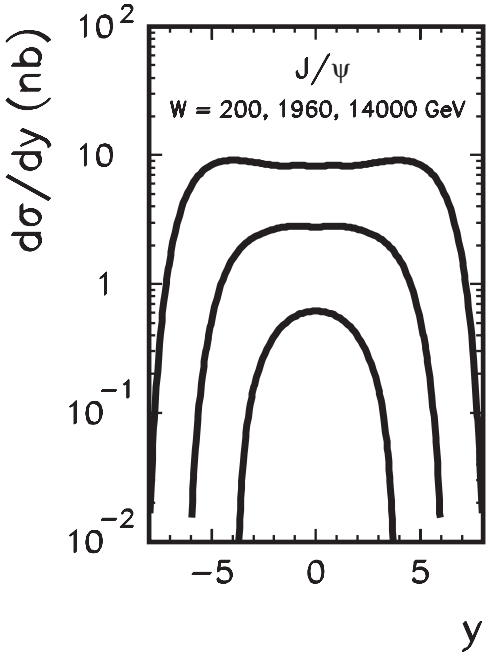

FIG. 5. $d\sigma/dy$ for exclusive J/ψ production as a function of y for RHIC, Tevatron, and LHC energies. No absorption corrections were included here.

positive rapidities, so that, for example, for the mechanism $\gamma\mathbb{P}$ it is the Pomeron exchange which "propagates" over the larger distance in rapidity space. It would be interesting to confront our present simple predictions with the predictions of the approach which uses unintegrated gluon distributions—objects which are/were tested in other high-energy processes. This will be the subject of our forthcoming studies.

Up to now we have not taken into account any restrictions on t_1 and/or t_2. In practice, it can be necessary to impose upper cuts on the transferred momenta squared. It is also interesting in the context of searches for the odderon to see how quickly the cross section for the "background" drops with t_1 and t_2. In Fig. 7 we show the distribution in J/ψ rapidity for different cuts on t_1 and t_2. Clearly, imposing a cut on t_1 and t_2 removes the photon-pole contribution dominant at small momentum transfers. Even a relatively small cut lowers the cross section considerably, and the dropping of the cross section is much faster than for the pomeron-odderon exchanges [12]. Imposing upper cuts on t_1 and t_2 will therefore help considerably to obtain a possible "odderon-enriched" sample. We wish to repeat here that without absorption effects the rapidity distributions of J/ψ in proton-proton and proton-antiproton collisions are identical.

$$\frac{d\sigma(pp \to ppJ/\psi, W)}{dy} = \frac{d\sigma(pp \to p\bar{p}J/\psi)}{dy}. \quad (3.1)$$

It is interesting to stress in this context that it is not the case for the transverse momentum distribution of J/ψ, where

$$\frac{d\sigma(pp \to ppJ/\psi, W)}{d^2\boldsymbol{p}_V} \neq \frac{d\sigma(p\bar{p} \to p\bar{p}J/\psi, W)}{d^2\boldsymbol{p}_V}. \quad (3.2)$$

This is demonstrated in Fig. 8, where we see that, at small transverse momenta of the vector meson, the interference enhances the cross section in pp collisions and depletes it in $p\bar{p}$ collisions. It is a distinctive feature of the mechanism discussed here that vector mesons are produced with very small transverse momenta. The difference between proton-antiproton and proton-proton collisions survives even at large rapidities of J/ψ. When integrated over the J/ψ

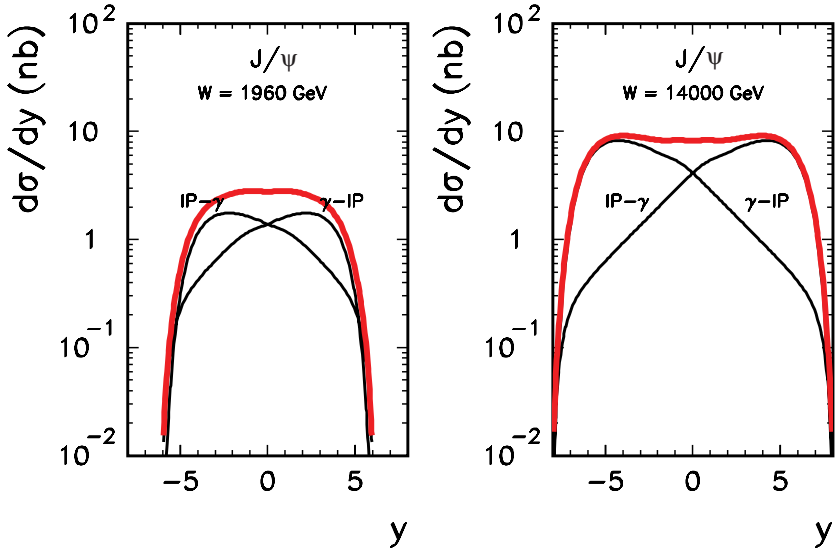

FIG. 6 (color online). $d\sigma/dy$ as a function of y for Tevatron and LHC energies. Individual processes are shown separately. Notice that the beam hadron h_1 of Fig. 1 moves at positive rapidities. No absorption corrections were included here.

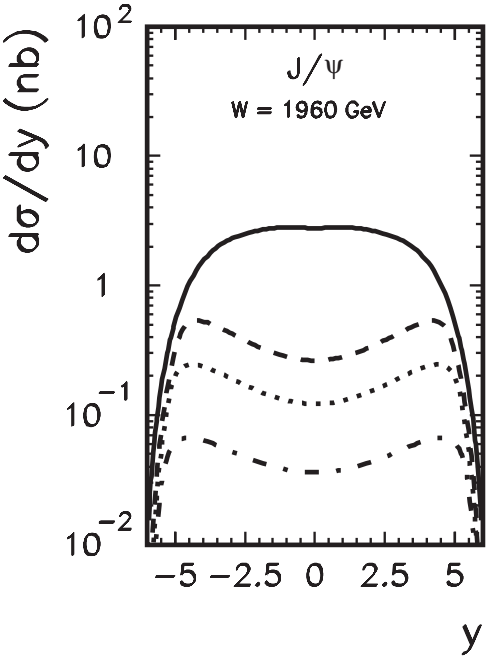

FIG. 7. $d\sigma/dy$ as a function of y for the Tevatron energy and different upper cuts on t_1 and t_2: $t_{\rm cut} = 0.0$ GeV^2 (solid line), $t_{\rm cut} = -0.05$ GeV^2 (thin solid line), $t_{\rm cut} = -0.1$ GeV^2 (dash-dotted line), and $t_{\rm cut} = -0.2$ GeV^2 (dashed line).

transverse momentum, and in the absence of absorptive corrections, cross sections will again be identical in the pp and $p\bar{p}$ cases.

B. Distributions of (anti)protons

Now we shall proceed to distributions related to (anti)-protons. In Fig. 9 we show distributions in the transferred momenta squared (identical for t_1 and t_2). We show separately the contributions of $\gamma\mathbb{P}$ and $\mathbb{P}\gamma$ exchanges. The figures clearly display the strong photon-pole enhancement at very small t.

In order to better understand the distributions in t_1 or t_2, in Fig. 10 we show how t_1 and t_2 are correlated. Here we do not make any restrictions on the rapidity range. The significant enhancements of the cross section in the form of ridges along $t_1 \sim 0$ and $t_2 \sim 0$ are again due to the massless photon exchange, and most of the integrated cross section comes from these regions. The pomeron-odderon and odderon-pomeron exchange contributions considered in Ref. [12] would not exhibit such significant local enhancements and would be smeared over a broader range in the (t_1, t_2) space. Therefore, in the dedicated searches for the odderon exchange, upper cuts on t_1 and t_2 should be imposed, and $t_{\rm upper} = -0.2$ GeV seems to be a good choice.

We repeat that the reaction considered in this paper leads to azimuthal correlations between the outgoing proton and antiproton. In Fig. 11 we show the corresponding angular distribution for the proton-antiproton collision (solid line). For reference we also show, by the dotted line, the incoherent sum of the $\gamma\mathbb{P}$ and $\mathbb{P}\gamma$ mechanisms. The distribution for proton-proton collisions (dashed line) is shown for comparison also at the Tevatron energy. Clearly the interference terms in both reactions are in opposite phases due to different electric charges of the proton and antiproton. In the absence of absorptive corrections, we have

$$\frac{d\sigma}{d\phi} = A \pm B\cos\phi \tag{3.3}$$

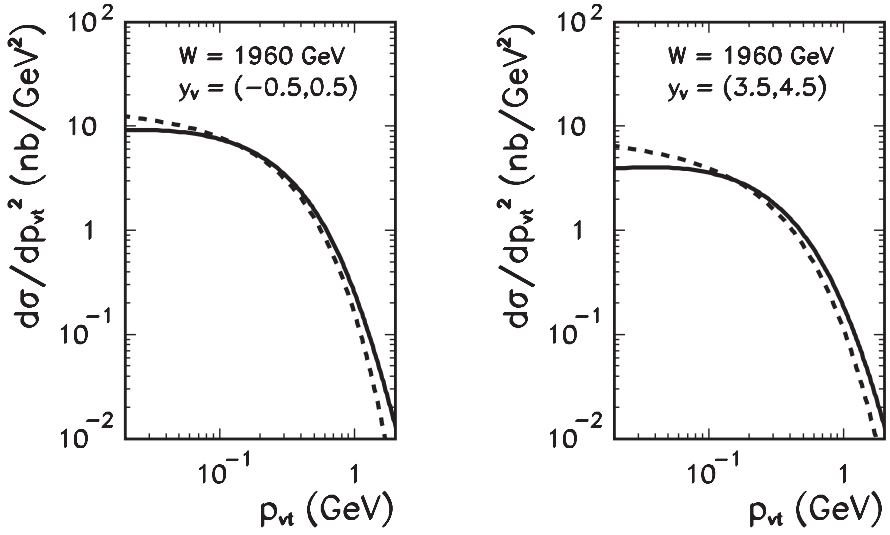

FIG. 8. The distribution $d\sigma/d\boldsymbol{p}_V^2$ of J/ψ as a function of J/ψ transverse momentum for different intervals of rapidity: $-0.5 < y < 0.5$ (left panel) and $3.5 < y < 4.5$ (right panel) at W = 1960 GeV. The result for pp collisions is shown by the solid line and the result for $p\bar{p}$ collisions by the dashed line. No absorption corrections were included here.

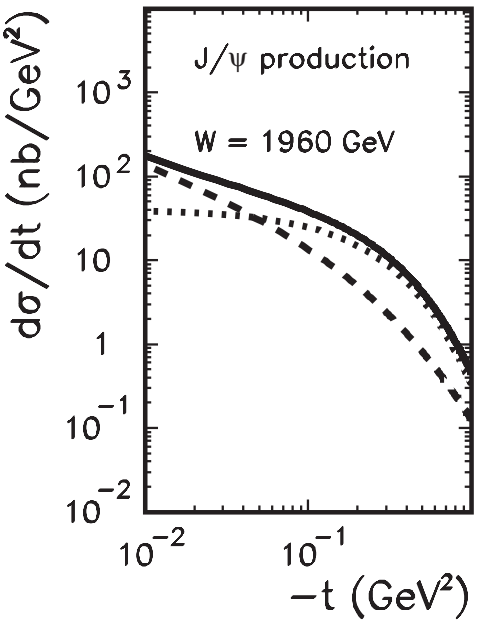

FIG. 9. $d\sigma/dt_{1/2}$ as a function of $t_{1/2}$ for W = 1960 GeV. In addition, the photon-exchange (dashed line) and pomeron-exchange (dotted line) contributions are shown. No absorption corrections were included.

for $pp(+)$ and $p\bar{p}(-)$ collisions, respectively. The interference effect (B/A) here is at the level of ~40%–50%.

In Fig. 12 we show the two-dimensional distributions differentially in both rapidity and azimuthal angle.

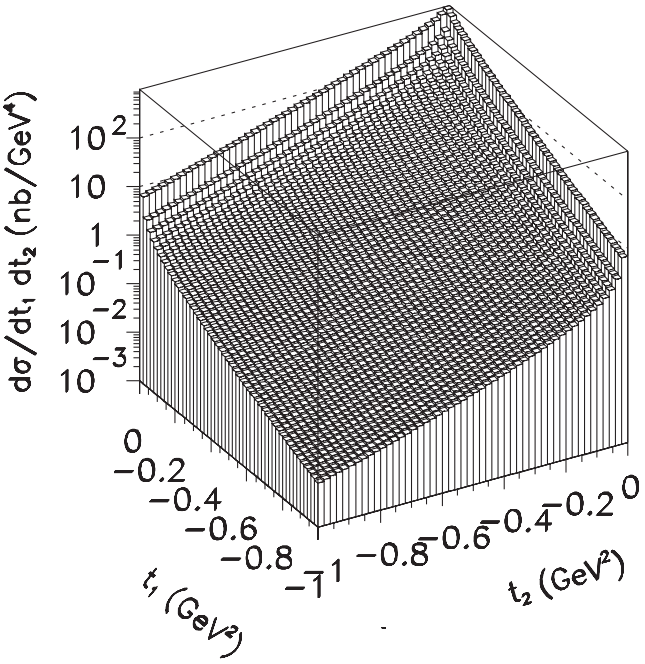

FIG. 10. Two-dimensional distribution in t_1 and t_2 for the Tevatron energy W = 1960 GeV. In this calculation a full range of the J/ψ rapidities was included. No absorption corrections were included here.

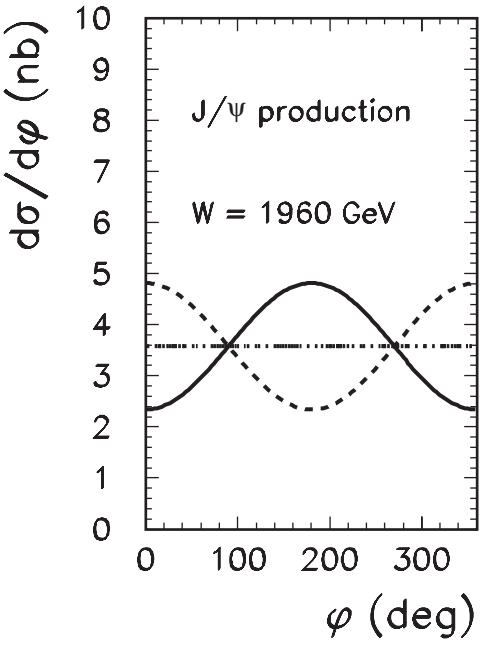

FIG. 11. $d\sigma/d\phi$ as a function of ϕ for W = 1960 GeV. The solid line corresponds to a coherent sum of amplitudes whereas the dashed line corresponds to an incoherent sum of both processes. No absorption corrections were included here.

Interestingly, the interference effect is significant over a broad range of J/ψ rapidity, which is reflected in the fact that even at large J/ψ rapidities one observes anisotropic distributions in the azimuthal angle.

Up to now we have considered only spin-preserving contributions. Now we wish to show the effect of the electromagnetic spin flip discussed in the previous section. In Fig. 13 we show the ratio of the helicity-flip to the helicity-preserving contribution. The ratio is a rather flat function of t_1 and t_2. At $t_1 = -1$ GeV^2 and $t_2 = -1$ GeV^2 the ratio reaches about 0.4.

C. Absorption effects

Now we will show the effect of absorptive corrections discussed in Sec. II B on various differential distributions.

Let us start from the presentation of the effects of absorption for selected points in phase space. In Fig. 14 we show the fully differential cross section $d\sigma/dydt_1dt_2d\phi$ as a function of ϕ for selected (fixed) values of t_1, t_2 and for $y = 0$. We show results for $p\bar{p}$ (left panel) and pp (right panel) collisions for the same center-of-mass energy $W = 1960$ GeV. While at smaller $t_{1,2}$ we observe a smooth reduction of the Born-level result, absorptive corrections induce a strong ϕ dependence at larger $t_{1,2}$. The positions of the diffractive minima which appear as a consequence of cancellations of the Born and rescattering amplitudes move with the value of $t \equiv t_1 = t_2$. In Fig. 15 we present the fully differential cross section as a function of t_1 and t_2 for $y = 0$ and $\phi = \pi/2$. For proton-

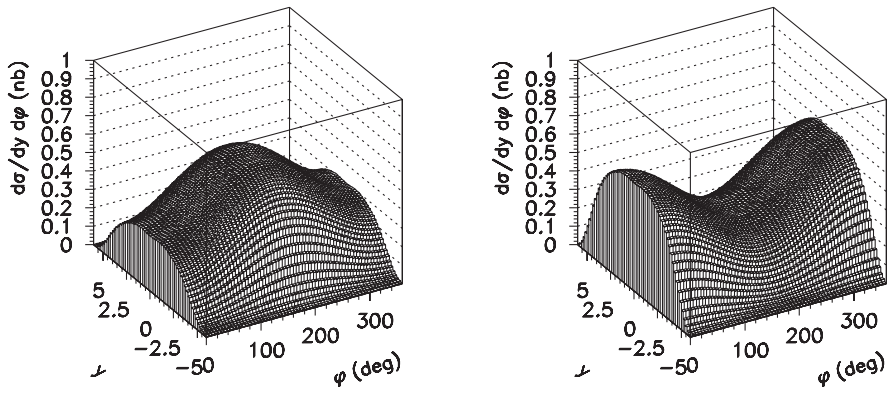

FIG. 12. $d\sigma/dyd\phi$ for W = 1960 GeV and for $p\bar{p}$ (left panel) and pp (right panel) collisions. No absorption corrections were included here.

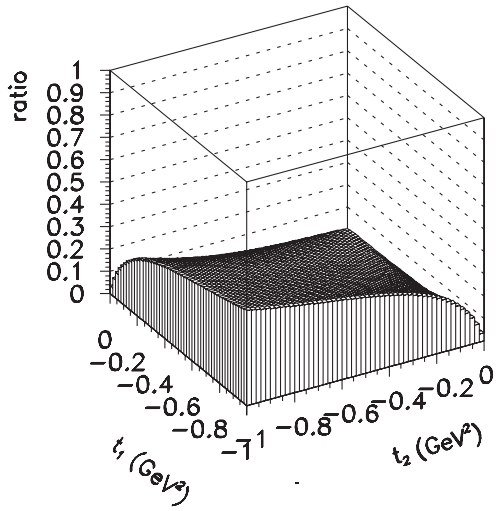

FIG. 13. The ratio of helicity-flip to helicity-preserving contributions as a function of t_1 and t_2.

proton scattering we clearly observe a diffractive minimum for $t_1 = t_2 \approx 0.4$ GeV^2. In Fig. 16 we show the fully differential cross section as a function of the transverse momentum squared $\boldsymbol{p}_1^2$ at a fixed value $\boldsymbol{p}_2^2 = 1$ GeV^2 at rapidity $y = 0$. The rich structure as a function of transverse momenta and azimuthal angles is also revealed by this plot. The plots in Fig. 17 give an idea, to which extent the diffractive dip-bump structure depends on the details of our treatment of absorption. Here we show, by the dotted line, the cross section calculated for the Born-level amplitude. The solid line shows the result with elastic scattering included, and for the dashed and dash-dotted lines we enhanced the rescattering amplitude T of Sec. II B by factors $\lambda = 1.2$ and $\lambda = 1.5$, respectively. The region of very small $\boldsymbol{p}_1^2$ is entirely insensitive to rescattering, reflecting the ultraperipheral nature of photon exchange. The diffractive dip-bump structure, situated at larger transverse momenta, reveals a dependence on the strength of absorptive corrections. This concerns the position of dips as well

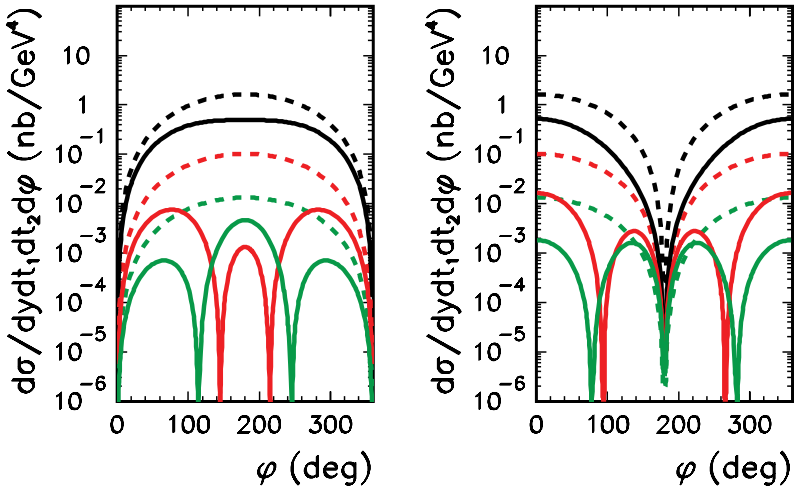

FIG. 14 (color online). Fully differential cross section $d\sigma/dydt_1dt_2d\phi$ as a function of ϕ for $y = 0$ and different combinations of $t_1 = t_2(-0.1, -0.3, -0.5$ GeV$^2)$ (from top to bottom) for $p\bar{p}$ (left panel) and pp (right panel) reactions. The solid lines include rescattering, while the dashed lines correspond to the Born-level mechanism only.

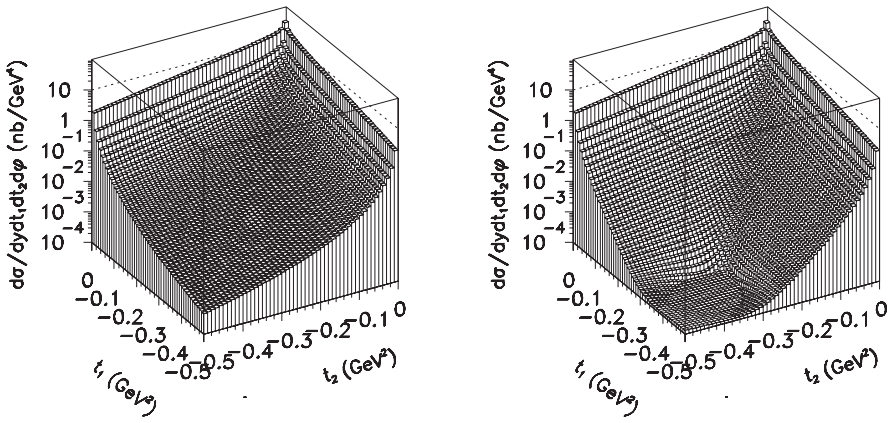

FIG. 15. The fully differential cross section $d\sigma/dydt_1dt_2d\phi$ as a function of t_1 and t_2 for $y = 0$ and $\phi = \pi/2$ for $p\bar{p}$ (left panel) and pp (right panel) reactions.

as the strength of the cross section in various windows of phase space.

The sensitivity to rescattering is, however, washed out in integrated observables—clearly the contribution from low transverse momenta, which is not strongly affected by rescattering, is large. This becomes apparent in Figs. 18–20.

In Fig. 18 we show the ratio of the cross section with absorption to that without absorption as a function of t_1 and t_2, again for $p\bar{p}$ (left panel) and pp (right panel). As a consequence of averaging over different phase-space configurations, the diffractive minima disappears. Again the plot reflects that, due to the ultraperipheral nature of the photon-exchange mechanism, absorption is negligible at very small $t_{1,2}$, and rises with t_1 and/or t_2. On average, absorption for the $p\bar{p}$ reaction is smaller than for the pp case.

It is important to stress again that the absorptive corrections in differential cross sections cannot be accounted for simply by a constant suppression factor, but they show a lively dependence over phase space. In Fig. 19 we show the differential cross section $d\sigma/dt$. The dashed line shows the

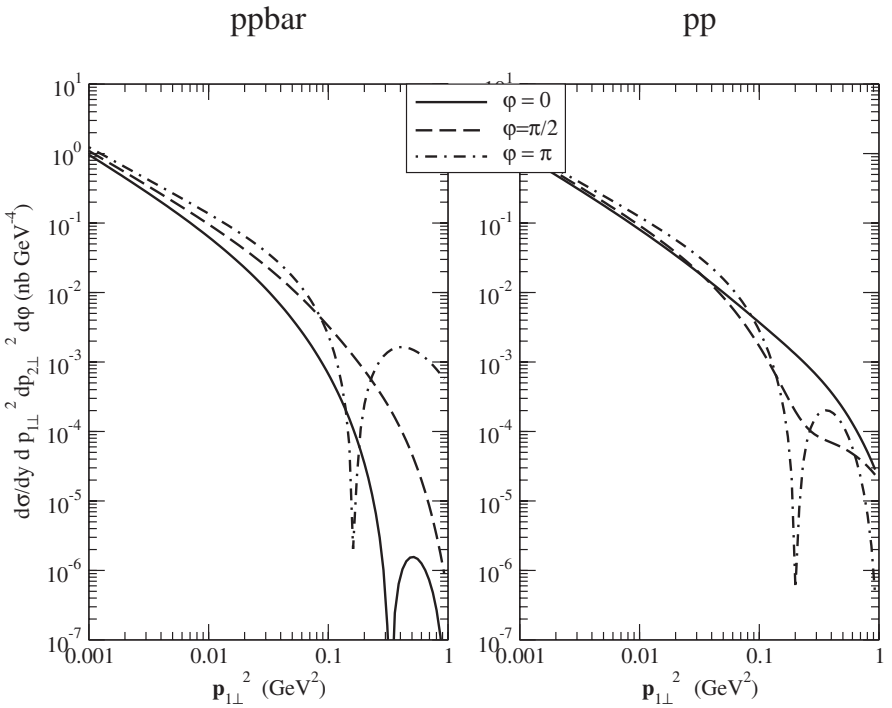

FIG. 16. Fully differential cross section $d\sigma/dyd\boldsymbol{p}_1^2d\boldsymbol{p}_2^2d\phi$ as a function of $\boldsymbol{p}_1^2$ at $y = 0$ and $\boldsymbol{p}_2^2 = 1$ GeV^2 for $p\bar{p}$ (left panel) and pp (right panel) collisions at W = 1960 GeV. Absorptive corrections (elastic rescattering) are included. Solid, dashed, and dash-dotted lines refer to different values of the azimuthal angle ϕ between outgoing (anti)protons.

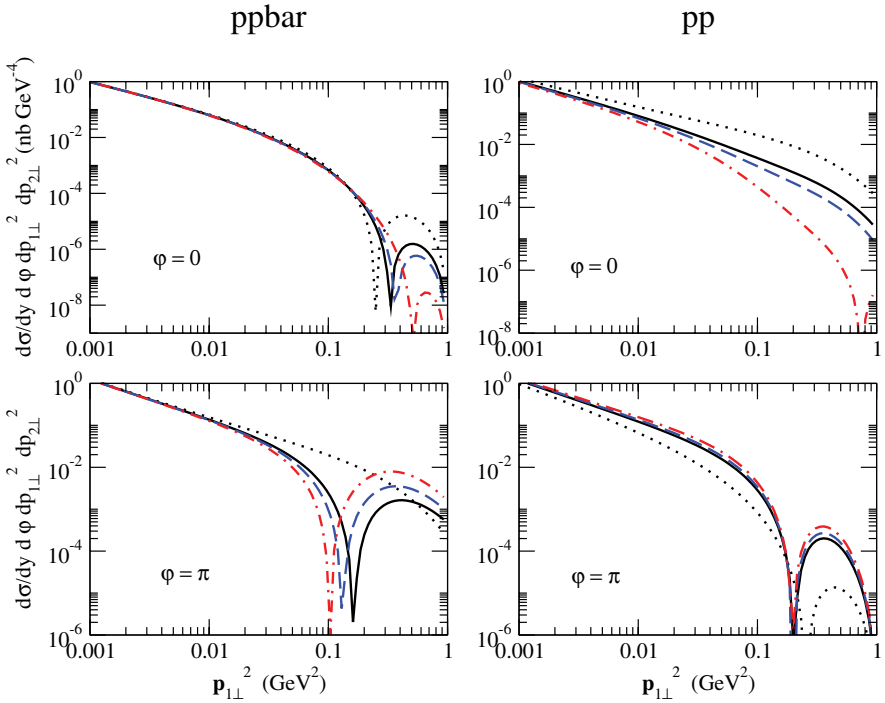

FIG. 17 (color online). Fully differential cross section $d\sigma/dyd\boldsymbol{p}_1^2d\boldsymbol{p}_2^2d\phi$ as a function of $\boldsymbol{p}_1^2$ at $y = 0$ and $\boldsymbol{p}_2^2 = 1$ GeV^2 for $p\bar{p}$ (left panel) and pp (right panel) collisions at W = 1960 GeV. The azimuthal angle ϕ is taken as $\phi = 0$ in the top row and $\phi = \pi$ in the bottom row. The dotted curve shows the Born-level cross section, without absorptive corrections included. The solid curve shows the result with elastic rescattering between (anti)protons included, while rescattering has been enhanced by a factor $\lambda = 1.2$ in the amplitude for the dashed curve, and by a factor $\lambda = 1.5$ for the dash-dotted curve.

result without absorption; the solid lines include absorptive corrections. They differ by a factor 1.5, by which rescattering has been enhanced in the lower curve. This enhancement of rescattering shows a modest effect, quite in agreement with the expectation mentioned above. The dependence of absorption on t is quantified by the ratio of full and Born-level cross sections shown by the dotted lines.

In Fig. 20 we show the suppression factor

$$\langle S^2(\boldsymbol{p}_V^2)\rangle = \frac{d\sigma^{\text{Born+Rescatt.}}/d\boldsymbol{p}_V^2dy}{d\sigma^{\text{Born}}/d\boldsymbol{p}_V^2dy}, \tag{3.4}$$

as a function of the J/ψ transverse momentum at $y = 0$. It is important to emphasize once more the strong functional dependence on $\boldsymbol{p}_V$, which is different for $p\bar{p}$ and pp

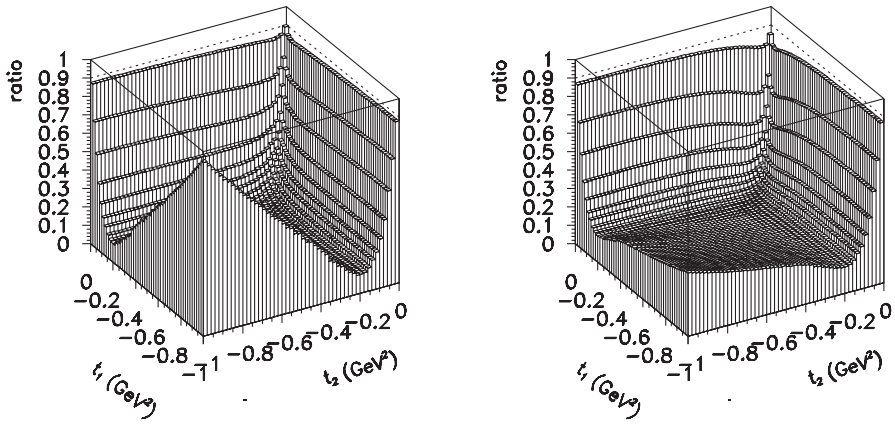

FIG. 18. The ratio of the cross sections with absorption to those without absorption for $p\bar{p}$ (left panel) and pp (right panel) scattering. Here the integration over y and ϕ was performed.

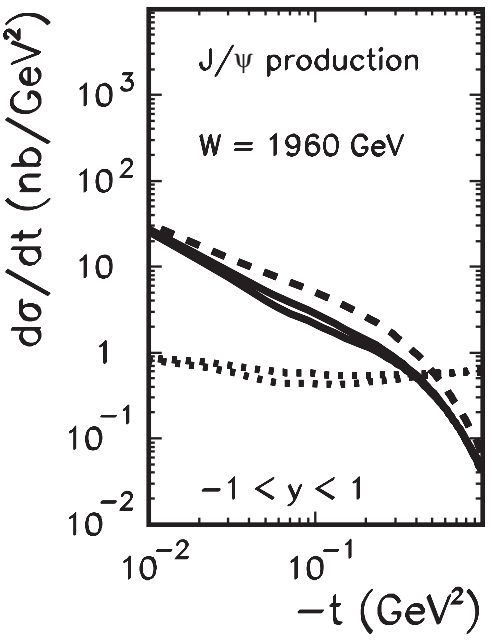

FIG. 19. Differential cross section $d\sigma/dt$, integrated over $-1 < y < 1$ for $p\bar{p}$ collisions. Dashed line: no absorptive corrections. Solid lines show the cross section with absorptive corrections included. Upper solid line: purely elastic rescattering. Lower solid line: rescattering enhanced by a factor $\lambda = 1.5$ in the amplitude. The dotted lines show the respective ratios $d\sigma^{\text{Born+Rescatt.}}/d\sigma^{\text{Born}}$.

collisions. Again, playing with the strength of absorption shows a modest effect.

The different behavior of absorptive corrections in pp and $p\bar{p}$ collisions is an interesting observation. It derives from the fact that rescattering corrections lift the cancellation of the interference term after azimuthal integration. Finally, let us comment on the expected reduction of rapidity distributions from absorptive corrections. These are, finally, rather flat functions of y. For the ratio

$$\langle S^2(y)\rangle = \frac{d\sigma^{\text{Born+Rescatt.}}/dy}{d\sigma^{\text{Born}}/dy}, \tag{3.5}$$

we obtain, in $p\bar{p}$ collisions,

$$\langle S^2(y=0)\rangle|_{p\bar{p}} \approx 0.9, \qquad \langle S^2(y=3)\rangle|_{p\bar{p}} \approx 0.8, \tag{3.6}$$

and for pp collisions,

$$\langle S^2(y=0)\rangle|_{pp} \approx 0.85, \qquad \langle S^2(y=3)\rangle|_{pp} \approx 0.75. \tag{3.7}$$

We note that this results in a small charge asymmetry,

$$\frac{d\sigma(p\bar{p})/dy - d\sigma(pp)/dy}{d\sigma(p\bar{p})/dy + d\sigma(pp)/dy} \approx 2 \div 3\%, \tag{3.8}$$

which derives entirely from absorptive corrections.

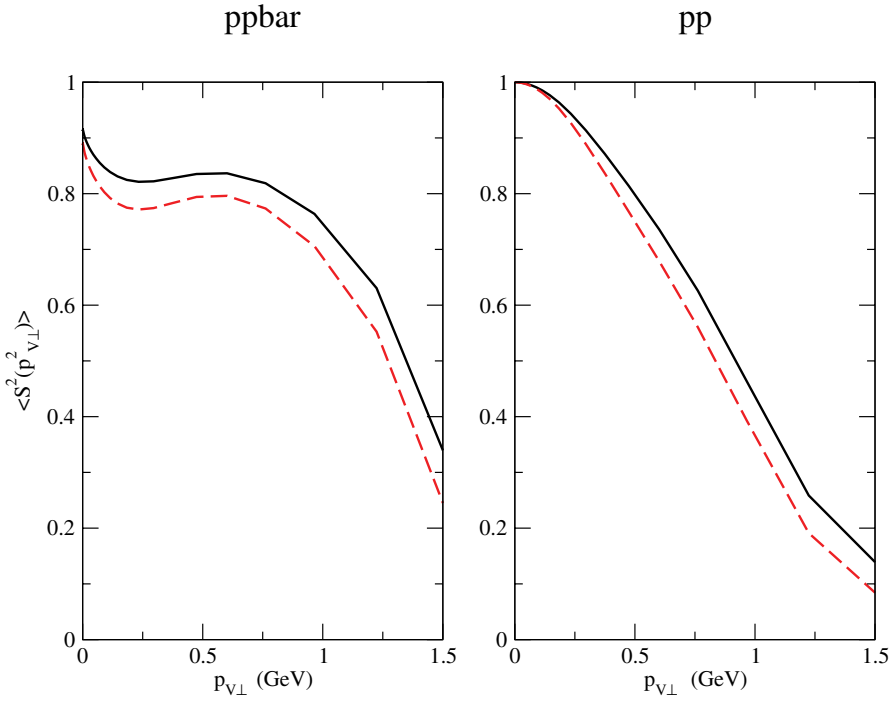

FIG. 20 (color online). The suppression factor $\langle S^2(\boldsymbol{p}_V^2)\rangle$ at $y = 0$ as a function of the J/ψ transverse momentum, for $p\bar{p}$ (left panel) and pp (right panel) collisions at W = 1960 GeV.

IV. CONCLUSIONS

In this paper we have calculated differential cross sections for exclusive J/ψ production via photon-pomeron ($\gamma\mathbb{P}$) and pomeron-photon ($\mathbb{P}\gamma$) exchanges at RHIC, Tevatron, and LHC energies. Measurable cross sections were obtained in all cases. We have obtained an interesting azimuthal-angle correlation pattern due to the interference of the $\gamma\mathbb{P}$ and $\mathbb{P}\gamma$ mechanisms. The interference effect survives over almost the whole range of J/ψ rapidities. At the Tevatron energy one can potentially study the exclusive production of J/ψ at the photon-proton center-of-mass energies 70 GeV $< W_{\gamma p} <$ 1500 GeV, i.e. in the unmeasured region of energies, much larger than at HERA. At the LHC this would be, correspondingly, 200 GeV $< W_{\gamma p} <$ 8000 GeV. At very forward rapidities this is an order of magnitude more than possible with presently available machines. Because of the photon pole, the differential cross section is concentrated in the region of very small t_1 and/or t_2. Imposing cuts on t_1 and t_2 lowers the cross section considerably. Electromagnetic helicity-flip processes play some role only when both $|t_1|$ and $|t_2|$ are large, that is, in a region where the hypothetical hadronic, odderon exchange contribution can also be present. It is a distinctive feature of the production mechanism that mesons are produced at very small transverse momenta, where the interference of $\gamma\mathbb{P}$ and $\mathbb{P}\gamma$ mechanisms induces a strongly different shape of the vector meson $\boldsymbol{p}_V^2$—distributions in pp vs $p\bar{p}$ collisions. We also estimated absorption effects on various distributions. In some selected configurations the absorptive corrections lead to the occurrence of diffractive minima. Naturally, the exact place of diffractive minima depends on the values of the model parameters, but they are washed out when integrated over the phase space or even its parts. Absorptive corrections for differential distributions are lively functions of transverse momenta, and cannot be accounted for simply by constant suppression factors. We have found that absorptive corrections induce a small charge asymmetry in rapidity distributions and total production cross sections. In the present paper we have concentrated on the exclusive production of J/ψ at energies $\sqrt{s} > 200$ GeV. The formalism used here can be equally well applied to exclusive production of other vector mesons, such as ϕ, Υ, as well as to the lower energies of e.g. the Facility for Antiproton and Ion Research, Japan Proton Accelerator Research Complex, and RHIC. For J/ψ production, recent parametrizations [30] of the photoproduction cross section from threshold to the highest energies may especially prove useful. We leave such detailed analyses for separate studies. The processes considered here are also interesting in the context of recently proposed searches for identifying the odderon. We find that the region of midrapidities ($-1 < y < 1$) and $t_1, t_2 < -0.2$ GeV^2 seems the best in searches for the odderon exchange. Should data reveal deviations from the conservative predictions given by us, a detailed differential analysis of both photon- and odderon-exchange processes, including their interference, in y, t_1, t_2, ϕ will be called upon.

ACKNOWLEDGMENTS

We thank Mike Albrow for useful comments regarding the experimental possibilities of exclusive J/ψ production at the Tevatron. We are indebted to Tomasz Pietrycki for help in preparing some figures. This work was partially supported by the Polish Ministry of Scientific Research and Information Technology, Grant No. 1 P03B 028 28.

APPENDIX

In Ref. [2] the differential cross section $\frac{d\sigma}{dt}$ for the reaction $\gamma^* p \to J/\psi p$ was parametrized as

$$\frac{d\sigma}{dt}(W, t, Q^2) = \frac{d\sigma}{dt}\Big|_{t=0, W=W_0} \left(\frac{W}{W_0}\right)^{4(\alpha(t)-1)} \times \exp(B_0 t)\left(\frac{m_{J/\psi}^2}{m_{J/\psi}^2 + Q^2}\right)^n, \tag{A1}$$

where $\alpha(t) = \alpha_0 + \alpha' t$. The values of the parameters found from the fit to the data are $\frac{d\sigma}{dt}|_{t=0, W=W_0} = 326$ nb/GeV^2, $W_0 = 95$ GeV, $B_0 = 4.63$ GeV^{-2}, $\alpha_0 = 1.224$, $\alpha' = 0.164$ GeV^{-2}, $n = 2.486$.

Assuming the dominance of the helicity-conserving transitions, and neglecting the real part, one can write

$$\mathcal{M}(s, t, Q^2) = \delta_{\lambda_\gamma \lambda_V} \delta_{\lambda_p \lambda_{p'}} i s \sqrt{16\pi \frac{d\sigma}{dt}|_{t=0, W=W_0}} \times \left(\frac{s}{W_0^2}\right)^{\alpha(t)-1} \exp(B_0 t/2)\left(\frac{m_{J/\psi}^2}{m_{J/\psi}^2 + Q^2}\right)^{n/2}, \tag{A2}$$

identical for each combination of particle helicities. In our case of hadroproduction the amplitude is a function of either (s_1, t_1, Q_2^2) or (s_2, t_2, Q_1^2).

[1] S. Chekanov *et al.* (ZEUS Collaboration), Eur. Phys. J. C **24**, 345 (2002).

[2] A. Aktas *et al.* (H1 Collaboration), Eur. Phys. J. C **46**, 585 (2006).

[3] I. Ivanov, N. N. Nikolaev, and A. A. Savin, Phys. Part. Nucl. **37**, 1 (2006).
[4] D. Barberis *et al.* (WA102 Collaboration), Phys. Lett. B **440**, 225 (1998); **432**, 436 (1998); **427**, 398 (1998); **397**, 339 (1997); **488**, 225 (2000).
[5] F. E. Close, G. R. Farrar, and Z. Li, Phys. Rev. D **55**, 5749 (1997); N. I. Kochelev, T. Morii, and A. V. Vinnikov, Phys. Lett. B **457**, 202 (1999); F. E. Close and G. A. Schuler, Phys. Lett. B **464**, 279 (1999); A. B. Kaidalov, V. A. Khoze, A. D. Martin, and M. G. Ryskin, Eur. Phys. J. C **31**, 387 (2003).
[6] V. A. Khoze, A. D. Martin, M. G. Ryskin, and W. J. Stirling, Eur. Phys. J. C **35**, 211 (2004).
[7] R. Pasechnik, A. Szczurek, and O. Teryaev, arXiv:0709.0857.
[8] A. Szczurek, R. Pasechnik, and O. Teryaev, Phys. Rev. D **75**, 054021 (2007).
[9] V. A. Khoze, A. D. Martin, and M. G. Ryskin, Phys. Lett. B **401**, 330 (1997);
[10] M. Boonekamp, A. De Roeck, R. Peschanski, and C. Royon, Phys. Lett. B **550**, 93 (2002); C. Royon, Acta Phys. Pol. B **37**, 3571 (2006).
[11] A. Schäfer, L. Mankiewicz, and O. Nachtmann, Phys. Lett. B **272**, 419 (1991).
[12] A. Bzdak, L. Motyka, L. Szymanowski, and J.-R. Cudell, Phys. Rev. D **75**, 094023 (2007).
[13] V. A. Khoze, A. D. Martin, and M. G. Ryskin, Eur. Phys. J. C **23**, 311 (2002).
[14] S. R. Klein and J. Nystrand, Phys. Rev. Lett. **92**, 142003 (2004); V. P. Goncalves and M. V. T. Machado, Eur. Phys. J. C **40**, 519 (2005).
[15] J. L. Pinfold, Proceedings of the International Conference on the Structure and Interactions of the Photon, Paris, 2007; R. Schicker, Proceedings of the 12th International Conference on Elastic and Diffractive Scattering, DESY, Hamburg, 2007.
[16] N. N. Nikolaev, Comments Nucl. Part. Phys. **21**, 41 (1992).
[17] J. D. Bjorken, Phys. Rev. D **47**, 101 (1993).
[18] B. Z. Kopeliovich, J. Nemchick, N. N. Nikolaev, and B. G. Zakharov, Phys. Lett. B **309**, 179 (1993); **324**, 469 (1994).
[19] N. N. Nikolaev and B. G. Zakharov, Z. Phys. C **49**, 607 (1991).
[20] J. Nemchik, N. N. Nikolaev, E. Predazzi, B. G. Zakharov, and V. R. Zoller, Zh. Eksp. Teor. Fiz. **113**, 1930 (1998) [J. Exp. Theor. Phys. **86**, 1054 (1998)].
[21] I. P. Ivanov, N. N. Nikolaev, and W. Schäfer, Phys. Part. Nucl. **35**, S30 (2004).
[22] V. A. Abramovsky, V. N. Gribov, and O. V. Kancheli, Yad. Fiz. **18**, 595 (1973) [Sov. J. Nucl. Phys. **18**, 308 (1974)]; A. Capella and A. Kaidalov, Nucl. Phys. **B111**, 477 (1976); L. Bertocchi and D. Treleani, J. Phys. G **3**, 147 (1977).
[23] N. N. Nikolaev and W. Schäfer, Phys. Rev. D **74**, 074021 (2006).
[24] V. N. Gribov, Zh. Eksp. Teor. Fiz. **56**, 892 (1969) [Sov. Phys. JETP **29**, 483 (1969)].
[25] F. Abe *et al.* (CDF Collaboration), Phys. Rev. D **50**, 5518 (1994).
[26] B. Z. Kopeliovich, N. N. Nikolaev, and I. K. Potashnikova, Phys. Rev. D **39**, 769 (1989).
[27] K. A. Ter-Martirosyan, Yad. Fiz. **10**, 1047 (1969) [Sov. J. Nucl. Phys. **10**, 600 (1970)].
[28] H. Kowalski and D. Teaney, Phys. Rev. D **68**, 114005 (2003); H. Kowalski, L. Motyka, and G. Watt, Phys. Rev. D **74**, 074016 (2006); M. Kuroda and D. Schildknecht, Phys. Lett. B **638**, 473 (2006).
[29] F. Yuan, Phys. Lett. B **510**, 155 (2001).
[30] R. Fiore, L. L. Jenkovszky, V. K. Magas, F. Paccanoni, and A. Prokudin, Phys. Rev. D **75**, 116005 (2007).